J Solid State Electrochem (2010) 14:1425–1443
DOI 10.1007/s10008-009-0957-4

ORIGINAL PAPER

Gold nanoparticle-modified glassy carbon electrode for electrochemical investigation of aliphatic di-carboxylic acids in aqueous media

F. M. El-Cheick · F. A. Rashwan · H. A. Mahmoud · Mahmoud El-Rouby

Received: 3 April 2009 / Revised: 3 August 2009 / Accepted: 10 October 2009 / Published online: 19 November 2009

Abstract The electrochemical reduction of di-carboxylic acids; oxalic, succinic, malic, and tartaric have been studied on the gold nanoparticles modified electrode in aqueous media solution of 0.1 M KCl. Gold nanoparticle (Au_{NPs})-modified electrodes were prepared by the electrodeposition with cyclic voltammetric method onto glassy carbon electrode in acidic media. The surface morphology of the electrodeposited gold nanoparticles was examined by SEM. Also, the electrochemical properties of the prepared electrodes were investigated with different electrochemical techniques; cyclic voltammetry, chronoamperometry, and electrochemical impedance spectroscopy. Cyclic voltammetric, chronoamperometric, and electrochemical impedance spectroscopic techniques were used for investigating the electrochemical behavior of the particulate acids. The modification of the electrode with Au nanoparticles (Au_{NPs}) enables the appearance of cyclic voltammogram peaks completely clear and sharp for the acids under investigation in comparison with the poor behavior of them in absence of the modification. All acids undergo totally irreversible redox reaction in neutral and acid media. The cyclic voltammetric response of the investigated acids is sensitive to pH, as well as of the scan rate. Each acid has a different reduction peak position from the other acids depending on the structure of the acid undergo the electroreduction process. Further, the lowest unoccupied molecular orbital energies of the investigated acids have been theoretically evaluated and are compared with their electroreduction potential peaks.

F. M. El-Cheick · F. A. Rashwan · H. A. Mahmoud · M. El-Rouby (✉)
Chemistry department, Faculty of Science, Sohag University, 82524 Sohag, Egypt
e-mail: dr_mahmoudelrouby@hotmail.com

Keywords Electrodeposition · Gold nanoparticles · Electroreduction · Di-carboxylic acids

Introduction

Nanoparticles can display four unique advantages over macroelectrodes when used for electroanalysis: enhancement of mass transport, catalysis, high effective surface area, and control over electrode microenvironment. Therefore, much work has been carried out into their formation, characterization, and employment for the detection of many electroactive species [1–5]. Metallic gold is one of the most malleable and ductile materials. It is soft but can be alloyed to increase its strength; it is unaffected by air and most reagents. Gold is a good conductor of heat and electricity. Gold nanoparticles are of wide interest as they display unusual optical, electronic, magnetic, and electrocatalytic properties from the bulk material [6]. Also, soft gold coatings are extensively applied for corrosion protection and to provide surfaces suitable for bonding. The electrodeposition of metal nanoparticles onto carbon electrodes has been widely studied [7–12]. Carbon electrodes are characterized by their high chemical inertness as well as low oxidation rate in addition to small gas and liquid permeability [13]. These properties render the glassy carbon electrode (GCE) to be a suitable substrate material for the loading of various metals and polymer thin films onto its surface aiming to improve its electrocatalytic activity toward the electrochemical reactions [14–16]. Electrochemical deposition conditions of metal are easy to alter, enabling creation of a wide range of electrodes with nanoparticles of differing sizes, shapes, and distributions. The procedure is rapid, simple, and reproducible, more than viable alternative

to the time-consuming and delicate production of an electrode via colloidal gold [17]. In this study, the electrodeposition of gold nanoparticles produced during the electroreduction of AuCl complex in acid solutions which has a much enhanced surface at room temperature (~298 K). The surface properties depend on the gold electrodeposition conditions, in particular, solution concentration, deposition potential, and other factors that have been discussed in this paper. The modified electrodes were characterized with different tools as SEM, cyclic voltammetry (CV), chronoamperometry (CA), and electrochemical impedance spectroscopy (EIS) techniques. Catalytic activity is one of the most important properties of Au_{NPs} so it is used to enhance the reaction efficiency towards the acids under investigation. Cathodic reduction of carboxylic acids should be performed with careful selection and control of electrolyte, temperature, pH, and electrode material and surface area of the electrode. Recently, it was found that: the cathodic reduction of a carboxyl group can give the carboxylate anion, the aldehyde, the alcohol, or the hydrocarbon in one-, two-, four-, or six-electron reduction, respectively [18]. The product of the electroreduction depends on the structure of the carboxylic acid, the electrode material, and the surface area. Such as, oxalic can be reduced to glyoxylic acid using high hydrogen overvoltage metal [19]. Also, the reduction of carboxylic acids has been categorized according to reaction mechanism and their p*K*a in dimethyl sulfoxide at platinum electrodes [20].

Experimental

Chemicals

All of acids: malic, tartaric, and succinic acids were purchased from BDH:

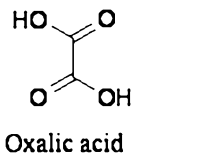

Oxalic acid

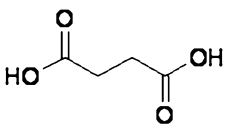

Succinic acid

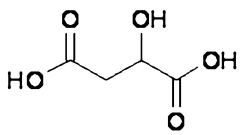

Malic acid

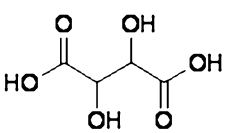

Tartaric acid

A 0.1-M potassium chloride (BDH), a 0.5-M Na2SO4 (BDH), a 0.1-M potassium nitrate (BDH), and a stock 0.1-M of potassium hexacyanoferrate (III) (BDH) solutions were freshly prepared by dissolving the required amounts in bi-distilled water. A 0.1×10−3-M and 0.8×10−3-M solution of hydrogen tetrachloroaurate (sms) were freshly prepared by dissolving the appropriate amount in a 0.5-M H2SO4.

Apparatus

All electrochemical experiments were performed with an EG&G PARC potentiostat/galvanostat model 273. The electrochemical software Model 273 A is controlled via IEEE 488 GPIB using IBM computer. EIS measurements were performed with a frequency response detector (amplifier) (Model 5208) driven by a potentiostat/galvanostat apparatus (model 273) from EG&G Instruments. The electrochemical software of this model is 378. A conventional three-electrode cell system was used, consisting of a bare or modified glassy carbon (3 mm in diameter) as a working electrode, platinum sheet as an auxiliary electrode. All potentials of all experiments were referred to the Ag/AgCl reference electrode. All experiments were carried out at thermostated temperature at 298±0.2 K. Surface analysis of the modified electrodes were carried out by using a JEOL JSM-5500 LV scanning electron microscope (JOEL, Japan), at an acceleration voltage of 15 keV and a working distance of 4 to 5 mm. Image analyses were performed visually and with common software (ImageJ, Wright Cell Imaging Facility, Toronto Western Research Institute, University Health Network) for particle counting and particle size. The energies of the molecular orbitals of the acids under investigation have been calculated using the program AM1 of winMOPAC 2.0.

Preparation of the modified electrode

Prior to the electrodeposition of Au nanoparticles, the glassy carbon electrode is polished first with no. 2000 emery paper, then with aqueous slurries of successively finer alumina powder with the help of polishing microcloth. Then, it was rinsed with double-distilled water. The bare GCE was then sonicated for 10 min in bidistilled water. Electrodeposition process was accomplished with cyclic voltammetry scanning between 0.90 and 0 V at a scan rate equal to 0.1 Vs−1 vs. Ag/AgCl from a fresh solution of 0.5 M H_2SO_4 containing 0.1×10^{-3} or 0.8×10−3 M of $HAuCl_4$ according to the required condition of the experiment. The delay time of the potential step was varied from 0 to 120 s to obtain Au deposits with

different characteristics, where the potential is delayed at the end of the cathodic peak for a definite time.

Results and discussion

Au nanoparticles electrodeposition

Au nanoparticles were electrodeposited on GCE from 0.5 M H2SO4 solution containing either 0.1×10−3 or 0.8×10−3 M HAuCl4 by applying cyclic voltammetry scanning between 0.90 and 0 V at a scan rate (ν) of 0.10 V s−1 as depicted in Fig. 1. Different delay time and concentrations were also employed to obtain different characteristics of the deposited gold nanoparticles to obtain a convenient electrode for sensing.

Two irreversible CV reduction peaks for Au3+ are observed; an initial (shoulder) cathodic current at ~0.7 V and a sharp main peak at ~0.5 V which is corresponding to the reduction of Au (III) to Au (0). The initial wave at 0.7 V can be attributed to the reduction of adsorbed AuCl4−. This behavior has been observed previously [5, 21, 22]. It has been concluded that the reduction of the adsorbed [AuC14]− complex ion at solid electrodes in both aqueous and nonaqueous solvents is a three-electron transfer process leading directly to the formation of gold metal with no obvious indication of an intermediate gold(I) complex [23]. The increase of the delay time from 0 to 120 s during the electrodeposition process increases slightly the cathodic peak current. Therefore, the primary nucleation of the particles increases (particle growth) along with the formation of new nucleation active sites commences. Thus, the particle size increases, but to less extent than that of the first case. This is confirmed with SEM. The modification of the electrodes were characterized and examined with different tools.

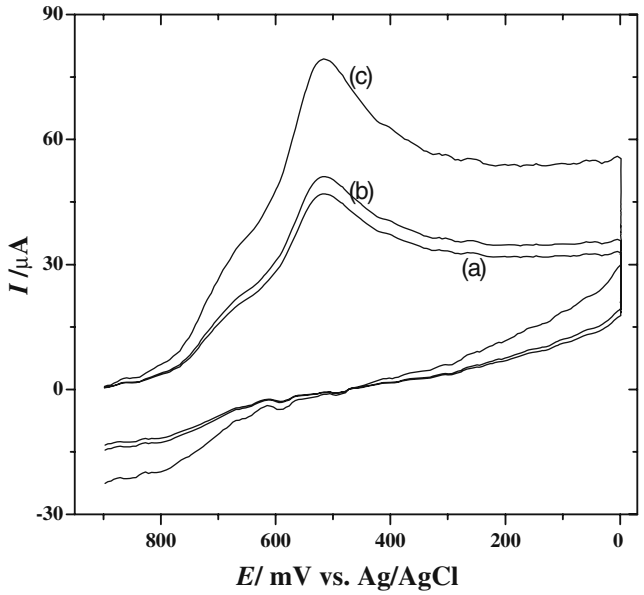

Fig. 1 CV of *a* 0.1×10^{-3}M and delay time 0 s, *b* 0.1×10^{-3}M and delay time 120 s, *c* 0.8×10^{-3}M and delay time 0 s of $HAuCl_4$ in 0.5 M H_2SO_4 at polished GCE and ν=0.100 Vs^{-1} at 298 K for the electroreduction of Au_{NPs}

Au nanoparticles characterization

SEM analysis characterization

Figure 2a–d shows the typical top view SEM images of the Au/GC under different conditions. The electrodeposited gold particles within the range of nanometer size and evenly distributed on the surface of GC Electrode.

The Au nanoparticles in the SEM images appear as circular, bright spots surrounded by a textured background of darker GC surface. It is clear from these images that the increase of either the delay time of deposition or the concentration of the $AuCl_4^-$ resulted in an increase in the average particle size of the Au nanoparticles [24]. Furthermore, as shown in Fig. 2b, the electrodeposition at low concentration (0.1 mM $AuCl^-$) yields a relatively high number density of particles. The calculated particles distribution is as following:

- 96% with size of ~2.8 nm
- other particles have 4 to 5 nm size range

At the higher concentration of the gold complex salt (0.8×10^{-3}M); low number density of relatively monodispersed particles are deposited with an increase of the particle size (mean value 37 nm). The particles are distributed as follow:

- ~68% of smaller size of ~27 nm
- ~10% of particles of ~37 nm
- 15% having a size of ~48 nm
- the others are ranged between 60 and 70 nm, as can be seen in Fig. 2c

The increase of the deposition time from 0.0 to 120 s leads to both increasing the size of the particle and of the particle number density, where the distribution of the particles is as follow:

- 76% of particles have ~9 nm
- 23% of the particles have 14–25 nm size range
- the other particles (1.2%) have size range of 35–60 nm, as shown in Fig. 2d

The nucleation growth is favored over the establishment of new deposition active sites; this occurs by increasing the

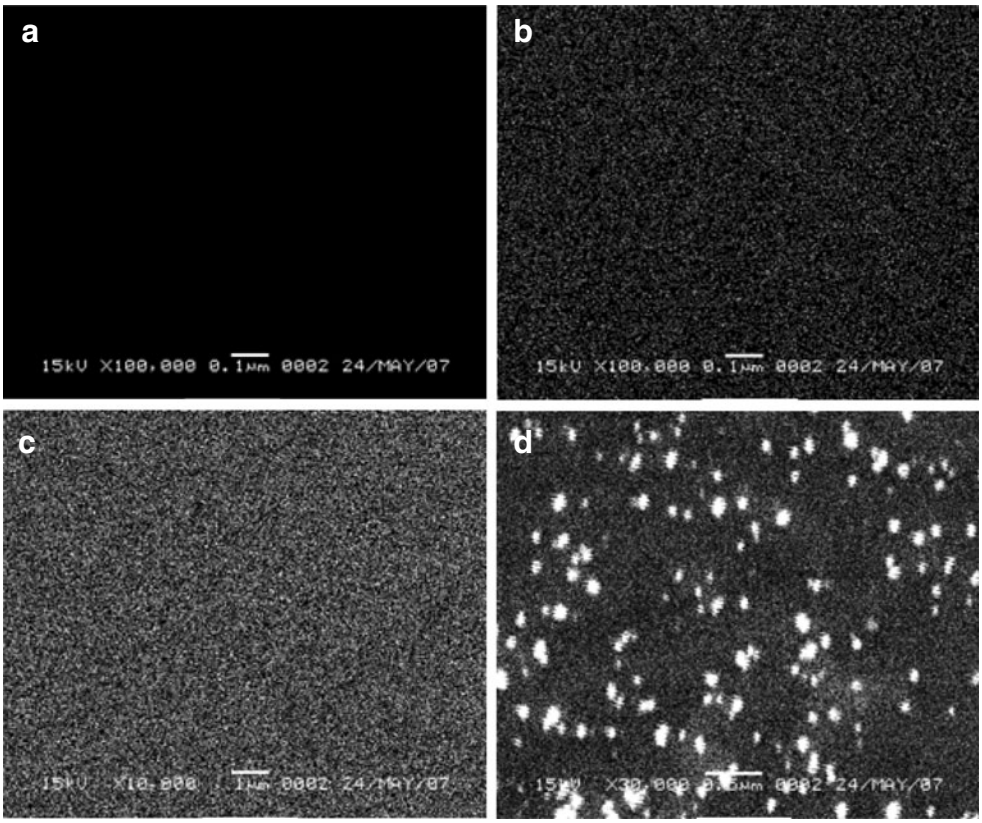

Fig. 2 SEM images of electrochemically deposited Au on GCE: **a** empty GCE, **b** delay time 0 s and 0.1×10^{-3}M, **c** delay time 120 s and 0.1×10^{-3} M, **d** delay time 0 s and 0.8×10^{-3}M

deposition time. The data of SEM image analysis of the modified electrode with nanoparticles are summarized in Table 1.

Further, the real surface area of the Au loading on GCE/cm^{-2} and the mass-specific surface area ($cm^2\,\mu g^{-1}$) reflect the catalytic properties of the modified electrodes, which were calculated by both SEM analysis and mass transfer method [25]. The data of the mass transfer method are almost in agreement with the data of SEM analysis for both the real surface area and for the mass-specific surface area ($cm^2\,\mu g^{-1}$). One may conclude that as the Au loading is increased, both the roughness factor and the real surface area increase; on the other hand, the mass-specific surface area decreases. These data have nearly similar behavior as in the literature [15, 26, 27]. Moreover, It has been found that the electroactive real surface area (*A*rsa) of the Au_{NPs}-modified electrode is of about 3.0–4.5 (roughness factor) times larger than that of the bare GC electrode (Table 1).

Table 1 Physical characteristics data determined from voltammetric measurements and SEM analysis for Au_{NPs}

Electrode	Q (μC)[a]	Au loading[b] (gcm^{-2})×10^5	Real surface area of Au loading[c] (cm^2)		Specific surface area[d] ($cm^2\,\mu g^{-1}$)		Roughness factor[e]	Mean diameter[f], nm
			SEM method	Mass transfer method	SEM method	Mass transfer method		
b	277.2	8.00	0.211	0.203	36.32	35.88	2.927	3
c	470.5	13.59	0.312	0.310	33.56	32.26	4.400	37
d	520.6	15.03	0.332	0.325	31.21	30.58	4.549	12

[a] Net cathodic charge passed in Au deposition

[b] Calculating Au loading assuming 100% current efficiency

[c] As estimated from SEM analysis and mass transfer methods

[d] Mass-specific surface area: surface area per unit weight of Au

[e] Surface area of Au per unit area of GCE

[f] Data measurement based on Imagej Program Software.

CV characterization

Cyclic voltammetry of electroactive species $Fe(CN)^{3-/4-}$ is a valuable tool for testing the kinetic barrier of the interface and is one of the most famous methods to estimate the real active surface area of the electrodes [28, 29].

Figure 3 presents the cyclic voltammetric measurements of 5×10^{-3}M $Fe(CN)6^{3-/4-}$ on both the bare and the modified GCE with gold nanoparticles, in 0.1 M KCl solution at a scan rate equal to 0.05 Vs^{-1}. Well-defined wave characterizing the cyclic voltammogram, obtained on the modified GCE where the peak-to-peak separation (ΔEp), is~0.085 V (Fig. 3, b–d). An obvious increase in anodic and cathodic peak currents is observed by decreasing the particle size deposits. This is due to high surface area enhancing the electron transfer. By case of using bare GCE, CVs are obtained with a peak-to-peak separation (ΔEp) of 0.318 V (Fig. 3, a), and a noticeable decrease in anodic and cathodic peak currents is observed compared with results obtained in case of the modified electrode. Thus, the electron transfer of the system was enhanced by modification of the GCE with the Au nanoparticles. Thus, the electron transfer of the system was improved after modification of the GCE with the Au nanoparticles. The peak currents of CV obtained from the modified electrodes (Fig. 3, b–d) is proportional to the square root of scan rate. This implies that these nanoparticles provided the necessary conduction pathways in promoting the electron transfer between the analyte and the electrode surface.

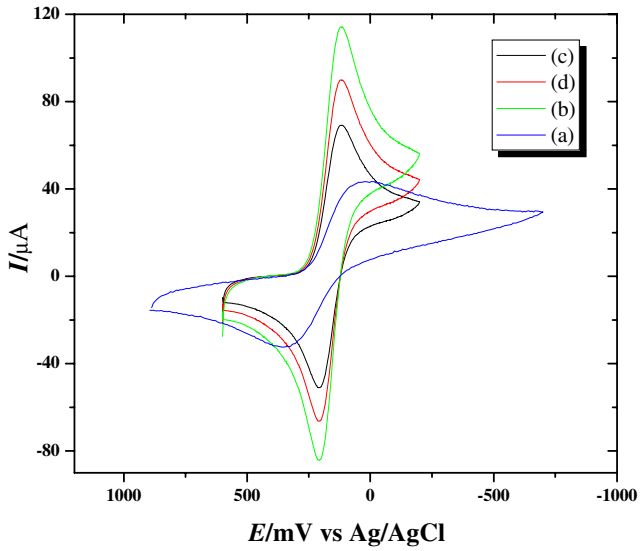

Fig. 3 CV of 5 mM $[Fe(CN)6]^{-3/-4}$ in 0.1 M KCl, at ν=50 mV s^{-1} at 298 K on bare (*a*) and modified GCE with Au_{NPs} at different loads; 8×10^{-5} (*b*), 13.59×10^{-5} (*c*), and 15.03×10^{-5}g cm^{-2} (*d*)

The real active surface area can be estimated by using Randles equation: [29, 30].

$$I_p = 3.01\times10^5 n^{3/2}\alpha^{1/2}D^{1/2}A_{rsa}c_0|\nu|^{1/2} \quad (1)$$

Where n is the number of electrons transferred in the redox reaction, ν the scan rate of the potential (V s^{-1}), Arsa the real surface area of the electrode (cm^2), D the diffusion coefficient of the species in the solution (cm^2s^{-1}) and calculated from chronoamperometric measurements (discussed later), c_0 the bulk concentration of the probe molecule in solution (mol cm^{-3}), and Ip the peak current of the redox couple (A).

The value of the electron transfer coefficient is assumed to be ≈0.5 for ferri/ferrocyanide redox couple. Heterogeneous charge transfer rate constant (ks) for this reaction, can be obtained according to the following equation [31]:

$$\psi = \frac{(D_0/D_R)^{\alpha/2}k_s}{\pi D_0\nu(nF/RT)^{1/2}} \quad (2)$$

By using the ΔE_p value and the working curve of Nicholson [32] to obtain the transfer parameter (ψ) and the heterogeneous charge transfer rate constant (ks) for the electron transfer process. The mean value of ks is found to be 6.8×10^{-4} and 1.08×10^{-3}cm s^{-1} on the modified electrodes and the GCE, respectively. This indicates to that the reaction is much faster on the modified electrodes and also reflects the facile nature of the charge transfer at the Au nanoparticle electrodes. The latter observation is predicted by the Marcus theory [33].

CA characterization

Chronoamperometry is a useful tool for the determination of the diffusion coefficients and investigating the kinetics of the charge transport on the modified electrodes. Figure 4 shows the chronoamperograms for the GCE/Au_{NPs} electrodes with different loads of Au in the presence of ferricyanide. The first and the second working electrode potentials are adjusted at 0.600 and 0.112 V (vs Ag/AgCl), respectively.

The diffusion coefficient can be obtained by using the relation between current decay and time as in Cottrell equation [31, 34]:

$$I = nFAD^{1/2}c_0\pi^{-1/2}t^{-1/2} \quad (3)$$

Where n is the number of electrons transferred, F the faraday constant (96,484 $Cmol^{-1}$), A the electrode surface area (cm^2), c_0 the bulk concentration (mol/cm^3), I the current (A), t the time elapsed (s), and D the diffusion coefficient (cm^2s^{-1}). The plots of I vs. $t^{-1/2}$ for different Au loadings gave straight lines, and the D mean value is ~$7.2\times10^{-6}cm^2s^{-1}$ for the ferricyanide ion [35].

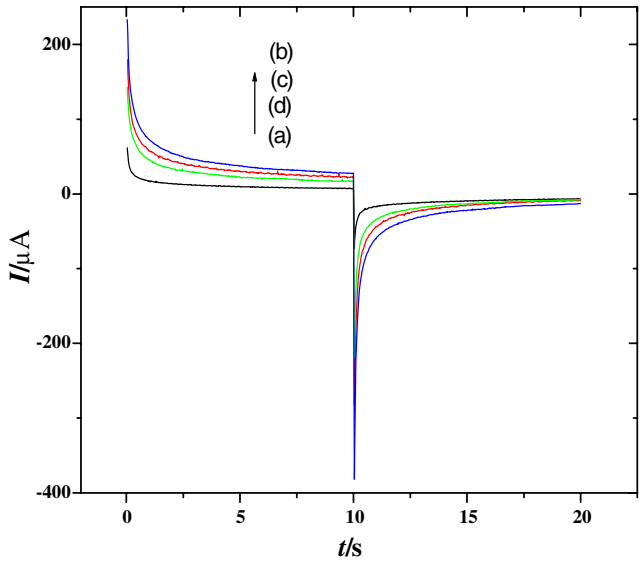

Fig. 4 Double step potential chronoamperograms obtained at bare (*a*) and modified GCE with Au_{NPs} for 5 mM $K_3[Fe(CN)_6]$ in 0.1 M KCl, at 298 K, at τ=10 s with different loads of ; 8×10^{-5} (*b*), 13.59×10^{-5} (*c*), and 15.03×10^{-5} g cm^{-2} (*d*)

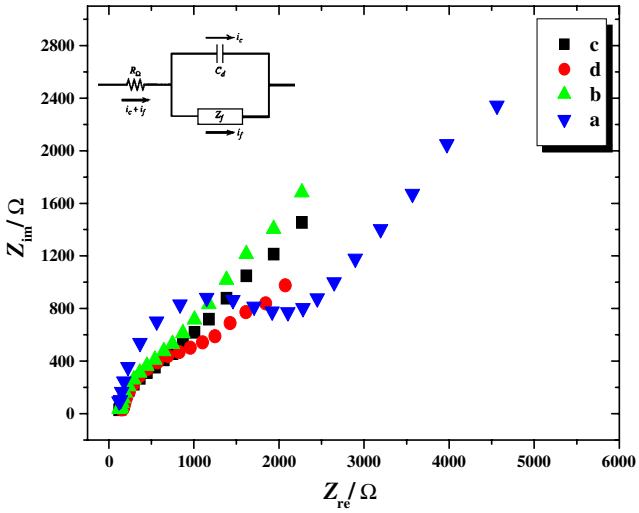

Fig. 5 Complex impendence plane plot for 5.0 mM $Fe(CN)_6^{3-/4-}$ in 1.0 M KCl. AC amplitude at 0.005 V, frequencies from 100 kHz to 5 Hz at 298 K. On bare (*a*) and modified GCE with Au_{NPs} with different loads of: 8.00×10^{-5} (*b*), 13.59×10^{-5} (*c*), and 15.03×10^{-5} g cm^{-2} (*d*), *Inset* (*left top*) is the Randle's equivalent circuit

The plots of $It^{1/2}$ vs. t for known concentration of ferricyanide show that $It^{1/2}$ function is constant and time-independent over a wide range of the experiment time. This is due to that the electron transfer process is under diffusion controlled. In addition, the catalytic rate constant (*k*cat) for ferricyanide on the GCE/Au_{NPs} has been calculated using Galus method, by applying equation [27]:

$$\frac{I_{cat}}{I_l} = \pi^{1/2}(k_{cat}c_0t)^{1/2} \quad (4)$$

Where I_{cat} is the catalytic current of ferricyanide on the modified electrode, I_l the limiting current in absence of ferricyanide, c_0 the bulk concentration (mol/cm^3), and t the time elapsed. The obtained mean value of k_{cat} is found to equal $32.28\times10^3\,M^{-1}s^{-1}$. This value points out to the high catalytic activity of the modified electrode towards the electroreduction of species.

EIS characterization

EIS is an effective and very sensitive method for probing the features of surface-modified electrodes [36–38] and to further investigate the impedance changes of the electrode surface on the modified electrodes. To investigate the electrical properties of the electrodes/solution interfaces, the Randle's equivalent circuit should be chosen in this case (Fig. 5).

Figure 5 demonstrates the EIS spectra presented as Nyquist plot for the bare GCE and for the modified electrodes of different loading Au nanoparticles for 5×10^{-3}M ferricyanide in 0.1 M KCl at the cathodic peak potential at 298 K. The charge transfer resistance (R_{ct}) at the electrode surface has a large value ~2,100Ω for the bare GCE in the test solution. The R_{ct} decreased dramatically to 500Ω when Au nanoparticles were deposited on the GCE electrode. When the Au loading of larger particle size increased, the *R*ct increased, and *R*ct decreased to ~500Ω (Fig. 5, b). This implies that the Au nanoparticles play an important role in the conductivity improvement, which facilitates the electron transfer.

At electrode (b), linear impedance (Warburg impedance, *Z*w) is observed with an angle of ~45° to the real axis at all frequencies. This behavior has been already assumed to be due to the presence of relaxation occurring at the electrode/solution interface and supports the diffusion controlled charge transfer process of the system. These data show that the Au nanoparticles are successfully working with high efficiency.

Electrochemical response of oxalic acid on the Au nanoparticle-modified electrode

CV

As shown in Fig. 6, typical cyclic voltammograms of oxalic acid were obtained in 0.1 M KCl at GCE and GCE modified with Au_{NPs}, one irreversible cathodic wave appeared at approximately −0.8 V (vs. Ag/AgCl) and a very small cathodic peak at approximately −0.55 V, the small peak may be attributed to the reduction of the dissociated proton of the oxalic acid. It has been known that in acid medium, the reaction begins with the reduction of protons. The reduced proton may be adsorbed on the surface of the electrode and reduced to the hydrogen atom, which can be exploited in the following electroreduction

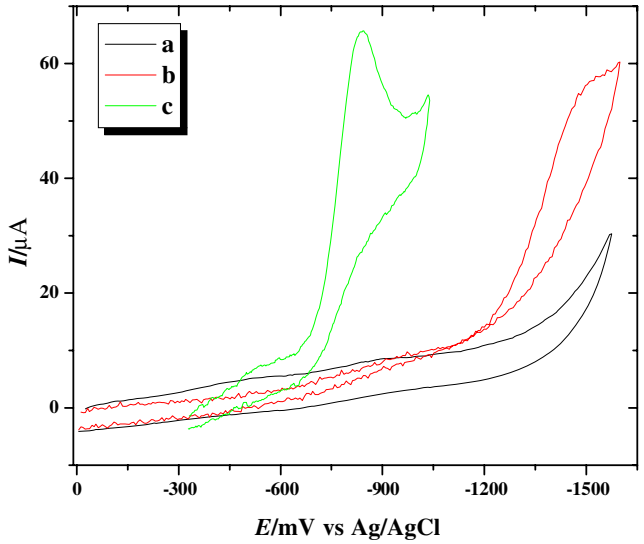

Fig. 6 CV of 1.25×10^{-3}M oxalic acid in 0.1 M KCl on bare GCE (*b*), modified GCE with Au_{NPs} in 0.1 M KCl only without oxalic acid (*a*) and modified GCE with Au_{NPs} at load of 8×10^{-5}g cm^{-2} in presence of 1.25×10^{-3}M oxalic acid (*c*), at ν=0.1 Vs^{-1} at 298 K

hydrogenation process, whereas no significant peaks appear at the bare GCE under the given potential limits. The cathodic peak potential *E*Pc, peak current, peak separation ($E_p-E_{p/2}$), and the current function $i_p/\nu^{1/2}$ for the electroreduction of oxalic acid on GCE modified with Au_{NPs} are summarized in Table 2.

Peak separations confirm that there is a totally irreversible two electron transfer process at the cathodic peak according to the relation [31, 32]:

$$\left|E_p - E_{p/2}\right| = \frac{1.857RT}{\alpha nF} = \frac{47.7}{\alpha n} \quad \text{mV} \tag{5}$$

In addition, there is a cathodic shift in peak potential or half peak potential of a bout ~33 mV (which approaches the theoretical value 30 mV for the irreversible reactions) for each tenfold increase in the rate of potential scan, ensuring the irreversibility of the system [31].

The linear responses obtained for $i_p-\upsilon^{1/2}$ relation reveals that the electron transfer process on the particular modified electrodes is controlled via diffusion phenomena. Furthermore, a linear increase in the peak height with the increase in concentration of the acid at millimolar levels (i.e., 1×10^{-3} to 8×10^{-3}M) is obtained. These data indicate also that the electron transfer processes are also controlled via diffusion phenomena. The criterion of the current function ($i_p/\nu^{1/2}$), which decreases with increasing the scan rate as shown in Table 2, ensures the presence of a chemical reaction following the electron transfer process (EC mechanism).

Heterogeneous charge transfer rate constant (k_s) for the electroreduction process can be obtained with the aid of Eq. 2. The value of k_s for the electroreduction of oxalic under the mentioned conditions, of amount ~0.25 cm s^{-1}, assuming $\alpha\approx0.5$, indicating that the reaction is much faster on the modified gold nanoparticles electrode and also reflect the facile nature of the charge transfer at the Au nanoparticle electrodes. One can conclude that by comparison of the voltammogram and the chemical structure of the investigated compound indicates that the cathodic wave potential is due to reduction of the carboxylic group of the acid.

Dependence of the I_{pc} and E_{pc} of Oxalic acid on the pH value The cyclic voltammetric behavior of oxalic acid was studied as a function of pH. The cyclic voltammograms show similar electrochemical characteristics as Fig. 6, c. The cathodic peak potential, E_{pc} shifts toward more negative potentials with an increase of pH while simultaneously diminishing in peak current (I_{pc}) height (Fig. 7a, b). The fact that the reduction wave decreases with the pH seems to indicate that the reduction of the radical is preceded by a protonation.

The number of protons that participate in the rate determining step can be calculated from the following equation:

$$\mathrm{d}E_p/\mathrm{d}(\mathrm{pH}) = mp \tag{6}$$

where *m* is the Tafel's slope and *p* the number of protons that participate in the rate determining step. Tafel's slope with respect to oxalic acid was obtained at potentials corresponding to the foot of the wave (i/i_p<0.05). It is found to be 32.5 mV/decade. Moreover, The variation of *E*p of the voltammograms with pH is a straight line with a slope of approximately −59.7 mV/pH indicating that during the electroreduction of oxalic acid on the GCE-modified Au_{NPs}, only two protons per acid molecule are consumed in the rate determining step (rds).

Table 2 Cyclic voltammetric data for the electroreduction of 1.25 mM oxalic acid on the GCE/ Au_{NPs} in 0.1 M KCl at 298 K

Scan rate (Vs^{-1})	$-E_p^c$ (V)	i_{pc} (μA)	$E_{p/2}-E_p$ (mV)	$i_p/\nu^{1/2}$ (μAmV^{-1} s$^{1/2}$)
0.05	0.776	55.70	44.10	7.8772
0.10	0.783	73.79	46.00	7.3788
0.20	0.789	102.60	47.00	7.2549
0.30	0.796	125.00	50.00	7.2169
0.40	0.803	137.02	50.50	6.8500
0.50	0.809	143.00	52.00	6.400

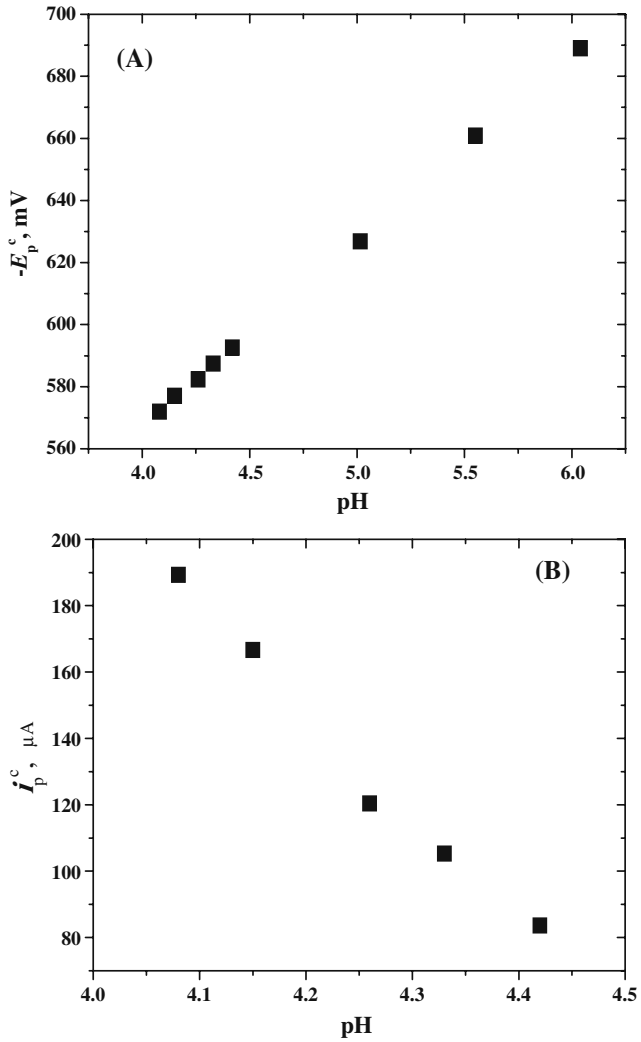

Fig. 7 Variation of the peak potential (**a**) and peak current (**b**) as a function of pH of (1.25 mM) oxalic acid in a universal buffer on modified GCE with Au_{NPs} at ν=100 mV^{-1} vs. Ag/AgCl

Therefore, the mechanism of oxalic acid reduction agree with that has been proposed, as follows [19, 39]:

$$HOOCCOOH + H^+ + e^- + M \rightarrow HOOCC(OH)_2M; \quad (7)$$

$$HOOCC(OH)_2M + e^- \rightarrow HOOCC(OH)^-_2 + M; \quad (8)$$

$$HOOCC(OH)^-_2 + H^+ \rightarrow HOOCCHO + H_2O; \quad (9)$$

where *M* represents the metal used as the cathode.

Double potential step CA

Chronoamperometry is one of the most important methods for the identification and determination of the EC mechanism and also for the determination of the rate of combined chemical and electrochemical reaction processes [40]. Therefore, this method is applied in the present study for the determination of the diffusion coefficient. It is known in chronoamperometric measurements that the i_a/i_c ratio should be equal to unity in absence but less than unity in the presence of chemical reaction.

Figure 8 shows the double potential step chronoamperograms of 1.25 mM oxalic acid on GCE modified with Au_{NPs} at 298 K at the cathodic peak of the acid. This figure reveals that the i_a/i_b ratio in the case of oxalic is less than unity in all cases. This may be due to the presence of follow-up chemical reaction after the charge transfer process (EC mechanism). Moreover, the diffusion coefficient can be obtained by using the relation between current decay and time as in Cottrell Eq. 3. The diffusion coefficient value of oxalic acid is of the order of $5.35 \pm 0.045 \times 10^{-5} cm^2 s^{-1}$ at 298 K.

Also the rate constant of the coupled chemical reaction (k_C) can be obtained by using the working curves (relation between I_a/I_b) as a function of $k\tau$ and $((t-\tau)/\tau)$ [41]. The rate of coupled chemical reaction (protonation) of oxalic acid at the cathodic peak after the electron transfer process is about ~0.205 s^{-1}. Furthermore, the plots of $It^{1/2}$ vs. t for the cathodic peak of oxalic show that $It^{1/2}$ is constant and time-independent. This assumes the diffusionally controlled electron transfer process.

EIS

Figure 9 shows the Nyquist plot of the impedance spectroscopy on the Au nanoparticles electrode for oxalic,

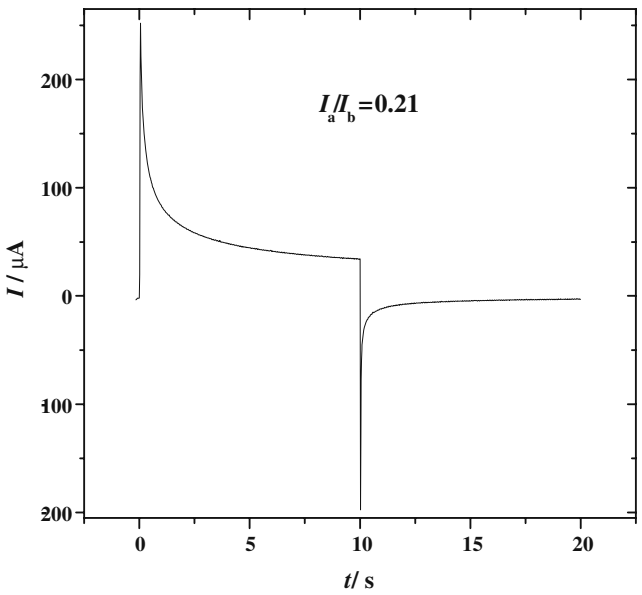

Fig. 8 Double potential step chronoamperogram obtained at GCE modified with Au_{NPs} at load of 8×10^{-5}g cm^{-2}, for 1.25×10^{-3}M oxalic acid in 0.1-M KCl, at *E*i=0 V, *E*s=−0.8 V and *E*f=0 V, at τ= 10 s, at 298 K

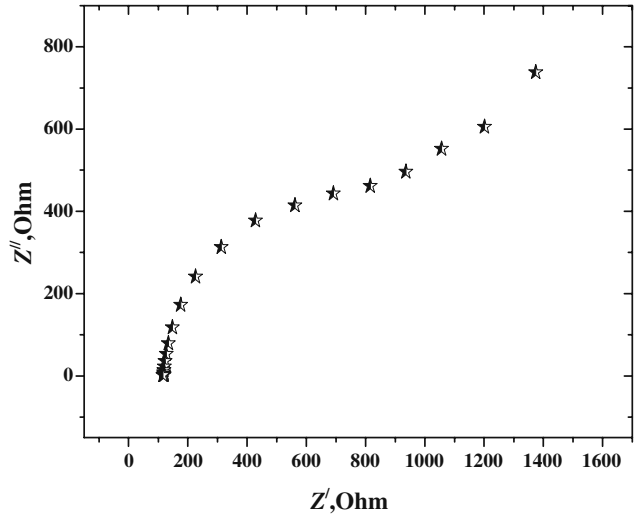

Fig. 9 Complex impedance plane plot at modified with Au_{NPs} at load of 8×10^{-5}g cm^{-2} for solution containing 1.25×10^{-3}M oxalic acid at the cathodic peak potential vs. Ag/AgCl, in 0.1-M KCl, AC amplitude at 0.005 V. The frequencies from 100 kHz to 5 Hz, at 298 K

measured from 6.31 Hz to 100 kHz at the cathodic potential peak for oxalic. The Randles equivalent circuit is not sufficient for the description of this case; thus, it should be assumed the presence of an additional impedance contribution connected with a coupled chemical reaction following the electron transfer process. The Ohmic resistance of solution (R_s), the charge transfer resistance (R_{ct}) at the electrode surface, and the double layer capacitance (C_{dl}) were obtained from Bode plot and listed in Table 3. The R_{ct} in the case of oxalic is considerably small and the C_{dl} relatively high. This can be interpreted on the basis that the electron transfer process in the electroreduction of oxalic acid is easy to occur. Moreover, the straight line at high frequency has not the unity slope. This reveals that the process is electron transfer combined with a chemical reaction (EC mechanism).

EIS measurement is a useful tool for the determination of the kinetic parameters of an electrochemical system [30, 42, 43]. Therefore, EIS is used for the determination of the heterogeneous rate of electron transfer, by using the reduced equation:

$$\cot\phi = 1 + \frac{\sqrt{D/2}}{k_s}\sqrt{\omega} \qquad (10)$$

Table 3 EIS data was obtained for the electroreduction of 1.25×10^{-3} M oxalic at the same conditions as in Fig. 8

Substance	R_s, Ω	R_{ct}, Ω	C_{dl} F×10^5	Φ Angel
Oxalic	118.85	551.00	7.08	46.90

Where ϕ is the phase angle, D the diffusion coefficient, assumed to be equal for both redox forms, k_s the heterogeneous rate constant of the electron transfer, and ω the angular frequency, assuming $\alpha=\beta=0.5$.

The dependence of the angular frequency (ω) on cot ϕ as in Fig. 10 shows that lot of points deviate from the detected line, and there are points arranged to form another straight line, indicating the presence of an EC process.

The heterogeneous rate of electron transfer reaction for the electroreduction of oxalic acid at the cathodic peak was obtained by this method, having value of ~0.0386 cm s^{-1}. This value is nearly consistent with that obtained from CV measurements and within the range of the diffusion-controlled processes confirmed with CV and CA measurements.

Electrochemical response of succinic acid on the Au nanoparticle-modified electrode

CV

As shown in Fig. 11, typical cyclic voltammograms of succinic acid were obtained in 0.1 M KCl at GCE and GCE modified with Au nanoparticles, two irreversible cathodic waves appeared at approximately −0.93 (main peak) and a small shoulder peak at −1.03 V (vs. Ag/AgCl). Whereas no significant peaks appear at the bare GCE under the given potential limits. The cathodic peak potentials E_{Pc}, peak currents, peak separations ($E_p - E_{p/2}$), and current functions $i_p/\nu^{1/2}$ for the electroreduction of succinic acid at different

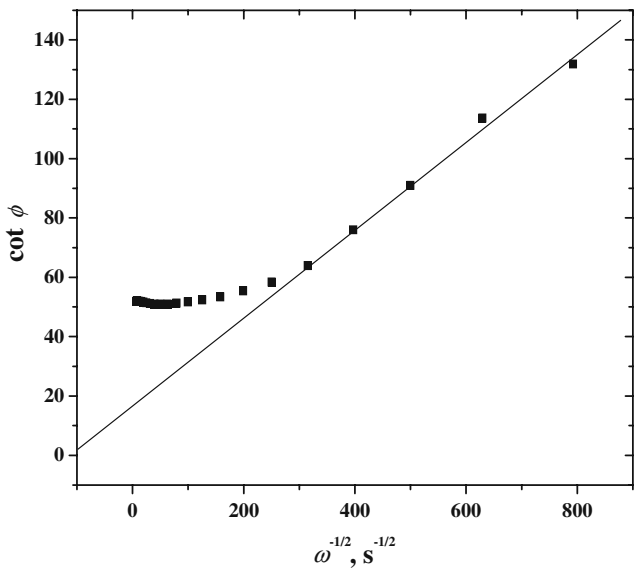

Fig. 10 Dependence of the faradic phase angel on the square root of angular frequency, derived from EIS data, for 1.25×10^{-3}M oxalic at the cathodic peak potential vs. Ag/AgCl, in 0.1 M KCl on Au_{NPs} at load of 8×10^{-5}g cm^{-2} at 298 K

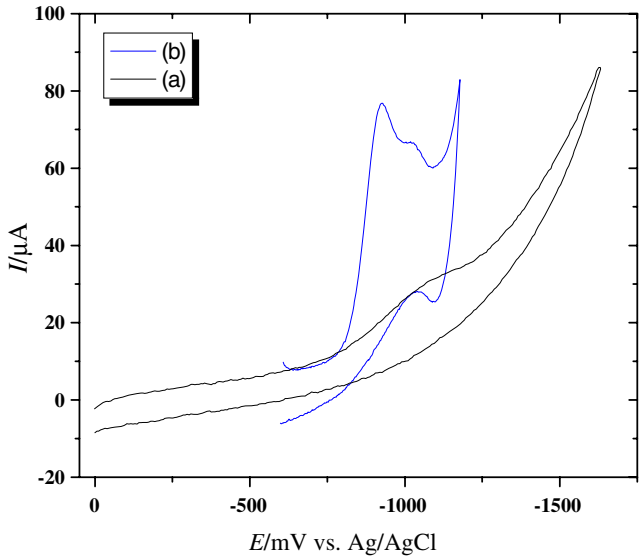

Fig. 11 CV of 1.25×10^{-3} M succinic acid in 0.1 M KCl on bare GCE (*a*) and modified GCE with Au_{NPs} at load of 8×10^{-5} g cm^{-2} (*b*), at ν= 0.1 Vs^{-1} at 298 K

scan rates at the first main cathodic peak on GCE modified with Au nanoparticles are summarized in Table 4.

Peak separations confirm that there is a totally irreversible two electron transfer process at the main cathodic peak according to the relation (Eq. 5). Also, there is a cathodic shift in half peak potential of about ~34 mV for each tenfold increase in the rate of potential scan. A linear increase relation between the peak current (I_P) and the square root of the scan rate reveals that the electron transfer process was controlled via diffusion phenomena. Also, a linear increase in the peak heights proportional to increase in concentrations of succinic acid at millimolar levels (i.e., 1×10^{-3} to 8×10^{-3}M) was observed. Similarly, it confirms that the electron transfer processes were also controlled via diffusion phenomena.

Current functions ($i_p/\nu^{1/2}$) decrease with increasing the scan rate (Table 4). This ensures that there is a chemical reaction along with the electron transfer process (EC mechanism). Thus, the electroreduction mechanism of

Table 4 CV data for the electroreduction of 1.25 mM succinic acid on the GCE/Au_{NPs} in 0.1 M KCl at 298

Scan rate (Vs^{-1})	$-Ep^c$ (V)	i_{pc} (μA)	$E_{p/2}-E_p$ (mV)	$i_p/\nu^{1/2}$ (μAmV^{-1} s$^{1/2}$)
0.05	0.928	42.10	46.0	5.95
0.10	0.935	57.80	50.2	5.78
0.20	0.942	74.34	54.3	5.26
0.30	0.949	87.70	55.6	5.07
0.40	0.956	99.70	57.8	4.98
0.50	0.962	110.43	59.3	4.93

succinic acid is similar to that of oxalic acid. This is due to a nearly similar chemical structure (free carboxyl group) and electrochemical behavior for both of them. But they are with a slight difference in the cathodic peak location, as it is shifted towards the negative direction in the latter case. This difference can be explained on the basis of the presence of the two methylene-$(CH_2)_2$-donating groups that hinder the process of electroreduction for succinic acid. Also, the difference in the chemical structure (methylene group) causes a difference in the values of pK_a of the acid.

Dependence of the I_{pc} and E_{pc} of oxalic acid on the pH value The cyclic voltammetric behavior of succinic acid was studied as a function of pH. The cyclic voltammograms show similar electrochemical characteristics as Fig. 11, b. The cathodic peak potential, E_{pc}, shifts toward more negative potentials with an increase of pH while simultaneously diminishing in peak current (I_{pc}) height (Fig. 12a, b). The fact that the reduction wave decreases with the pH seems to indicate that the reduction of the radical is preceded by a protonation. The number of protons that participate in the rate-determining step was calculated from Eq. 6. Tafel's slope with respect to succinic acid was obtained at potentials corresponding to the foot of the wave ($i/i_p<0.05$). It is found to be ≈32 mV/decade. On the other hand, the variation of E_p, with pH, linear with a slope of −60.37 mV/pH indicates that only two H^+ion per acid molecule reduced takes part in the rds. The electroreduction mechanism of succinic acid agrees with that has been proposed for oxalic acid.

Double potential step CA

Figure 13 shows the double potential step chronoamperograms at cathodic peak of succinic acid. This figure reveals that the I_a/I_b ratio in the case of succinic is less than the unity. This is due to the presence of electron transfer process followed by a chemical reaction (EC mechanism). The diffusion coefficient of succinic acid is of the order of 4.28×10^{-5} cm^2 s^{-1}.

The rate of coupled chemical reaction (protonation) of succinic acid at the first main cathodic peak after the electron transfer process is about ~0.20 s^{-1}. Also, the plots of $It^{1/2}$ vs. t for the cathodic peak of succinic show that $It^{1/2}$ is constant and time-independent. This assumes the diffusionally controlled electron transfer process.

EIS

Figure 14 shows the Nyquist plot of the impedance spectroscopy on the modified Au_{NPs} electrode for succinic, measured from 6.31 Hz to 100 kHz at the cathodic potential

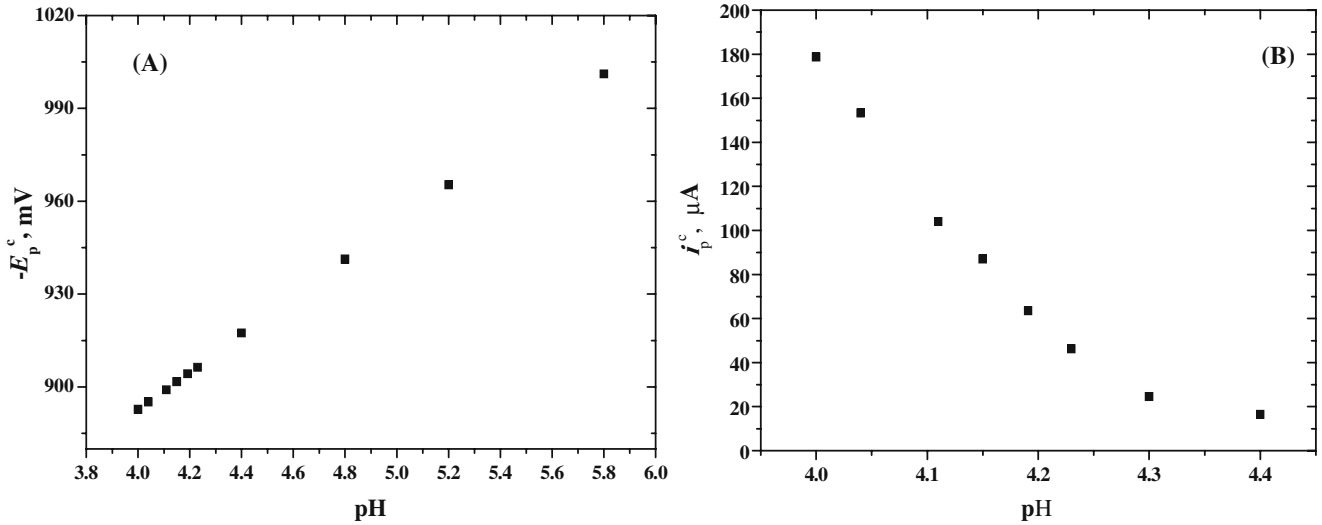

Fig. 12 Variation of the peak potential (**a**) and peak current (**b**) as a function of pH of (1.25×10^{-3}M) succinic acid in a universal buffer on modified GCE with Au_{NPs} at ν=0.10 V^{-1} vs. Ag/AgCl

peak for succinic. The Randles equivalent circuit is not sufficient for the description of this case; thus, it should be assumed the presence of an additional impedance contribution connected with a coupled chemical reaction following the electron transfer process.

The extracted parameters for the circuit elements are summarized in Table 5. The R_{ct} in the case of succinic acid is considerably small, but higher than oxalic acid, so the C_{dl} relatively high but less than oxalic. This can be interpreted on the basis that the electron transfer process in the electroreduction of succinic acid is easy to occur but less than oxalic acid. Moreover, the straight line at high frequency has not the unity slope. This reveals that the process is electron transfer combined with a chemical reaction (EC mechanism).

The dependence of the angular frequency on cot ϕ as in Fig. 15 shows that lot of points deviate from the detected line, and there are points arranged to form another straight line, indicating the presence of an EC process. The heterogeneous rate of electron transfer reaction for the electroreduction of succinic acid at the first cathodic peak was obtained, having value of ~0.0255 cm s^{-1}. This value is nearly consistent with those obtained from CV measurements and within the range of the diffusion-controlled processes confirmed with CV and CA measurements.

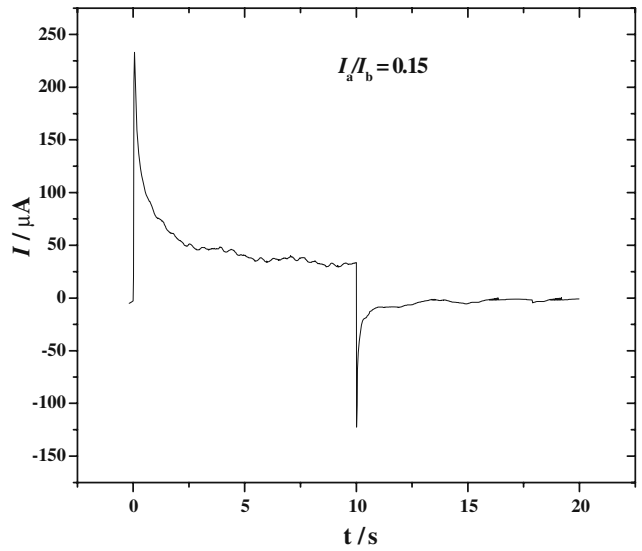

Fig. 13 Double potential step chronoamperogram obtained at GCE modified with Au_{NPs} at load of 8×10^{-5}g cm^{-2} for 1.25×10^{-3}M succinic acid in 0.1-M KCl, at Ei=0 V, Es=−0.93 V, and Ef=0 V, at τ=10 s, at 298 K

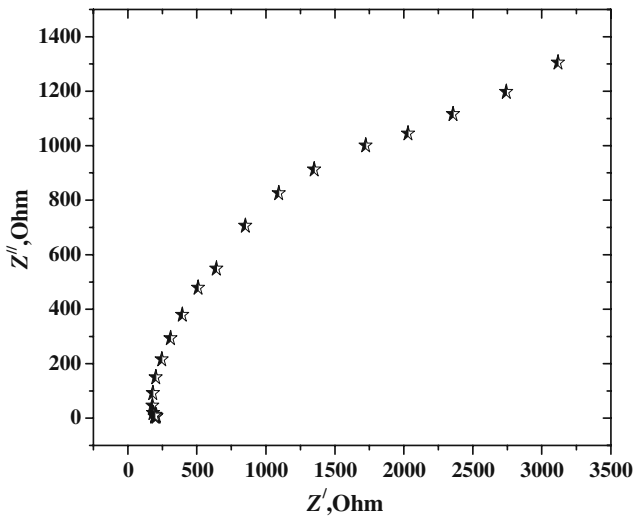

Fig. 14 Complex impedance plane plot at modified with Au_{NPs} at load of 8×10^{-5}g cm^{-2} for solution containing 1.25×10^{-3}M succinic acid at the cathodic peak potential vs. Ag/AgCl, in 0.1 M KCl, AC amplitude at 0.005 V. The frequencies from 100 kHz to 5 Hz, at 298 K

Table 5 EIS data was obtained for the electroreduction of 1.25×10^{-3} M succinic at the same conditions as in Fig. 14

Electrode	R_s, Ω	R_{ct}, Ω	C_{dl}F$\times10^{-5}$	Φ Angel
Au_{NPs}	199.50	1,314.00	5.37	46.82

Electrochemical response of malic acid on the Au nanoparticle-modified electrode

CV

Figure 16 shows the cyclic voltammograms of malic acid on the bare GCE and GCE/Au_{NPs} in a 0.1-M KCl solution. The electroreduction behavior of malic acid revealed a cathodic reduction peak potential (E_{pc}) at −0.88 V and a small cathodic peak at −0.74 V (vs. Ag/AgCl) (curve b). This small peak may be attributed to the reduction of the dissociated proton of as in the oxalic acid, whereas nearly no significant peaks appear at the bare GCE under the given potential limits. The cathodic peak potential E_{Pc}, peak current, peak separation ($E_p-E_{p/2}$), and current function $i_p/\nu^{1/2}$ for the electroreduction of malic acid on GCE modified with Au nanoparticles are summarized in Table 6.

Peak separations confirm that there is a totally irreversible two electron transfer process at the main cathodic peak according to the relation (Eq. 5). Also, there is a cathodic shift in peak potential of about ~32 mV for each tenfold increase in the rate of potential scan. A linear increase relation between the peak current (I_P) and the square root of the scan rate reveals that the electron transfer process was

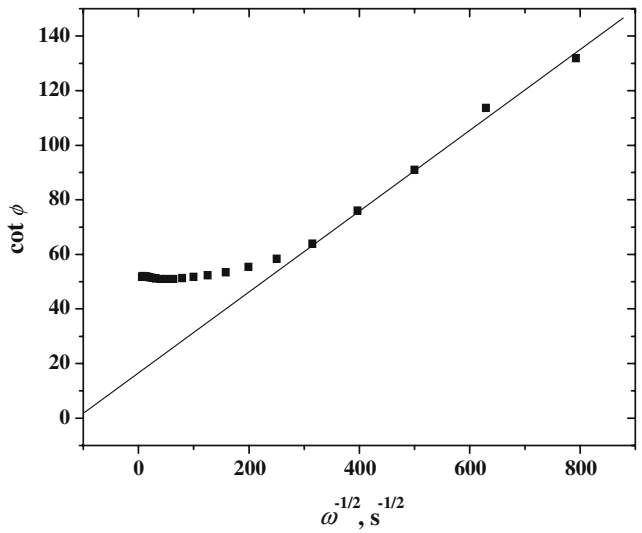

Fig. 15 Dependence of the faradic phase angel on the square root of angular frequency, derived from EIS data, was measured for 1.25×10^{-3}M succinic the cathodic peak potential vs. Ag /AgCl, in 0.1-M KCl at Au_{NPs} electrode at load of 8×10^{-5}g cm^{-2} at 298 K

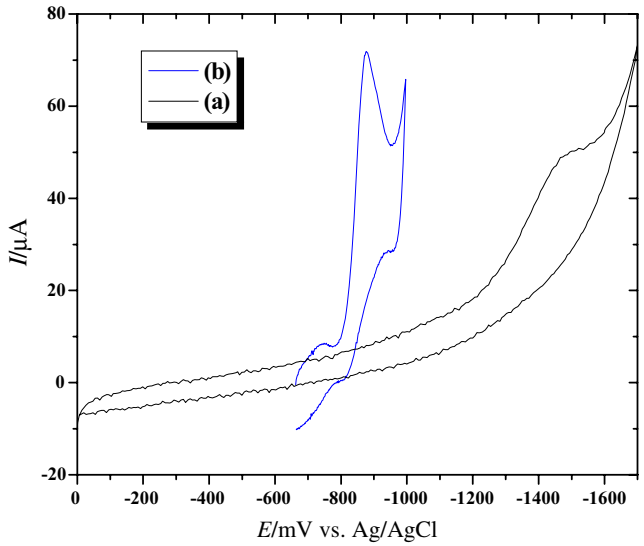

Fig. 16 CV of 1.25×10^{-3}-M malic acid in 0.1 M KCl on bare GCE (*a*) and modified GCE with Au_{NPs} at load of 8×10^{-5}g cm^{-2} (*b*), at ν= 0.1 Vs^{-1} at 298 K

controlled via diffusion phenomena. Also, a linear increase in the peak heights proportional to increase in concentrations of malic acid at millimolar levels (i.e., 1×10^{-3} to 8×10^{-3}M) was observed. Similarly, it confirms that the electron transfer processes were also controlled via diffusion phenomena. Current functions ($i_p/\nu^{1/2}$) decreases with increasing the scan rate (Table 6). This indicates that there is a chemical reaction companied with the electron transfer process (EC mechanism) at the electroreduction of malic acid.

Heterogeneous charge transfer rate constant (*k*s) for the electroreduction of malic acid can be obtained according to Eq. 2 and by using the mentioned method above. The value of *k*s for the electroreduction of malic under the mentioned conditions, amounts to ~0.1 cm s^{-1}, assuming $\alpha\approx0.5$ indicating that the reaction is much faster on the modified gold nanoparticles electrode and also reflect the facile nature of the charge transfer at the Au nanoparticles

Table 6 CV data for the electroreduction of 1.25 mM malic acid on the GCE/Au_{NPs} in 0.1 M KCl at 298 K

Scan rate (mVs^{-1})	$-Ep^c$ (V)	i_{pc} (μA)	$E_{p/2}-E_p$ (mV)	$i_p/\nu^{1/2}$ (μAmV^{-1}s$^{1/2}$)
50	0.842	39.40	29.27	5.5720
100	0.879	53.20	31.33	5.3200
200	0.892	72.70	31.67	5.1407
300	0.900	85.30	33.33	4.9248
400	0.907	95.00	34.00	4.7500
500	0.911	104.00	33.00	4.6510

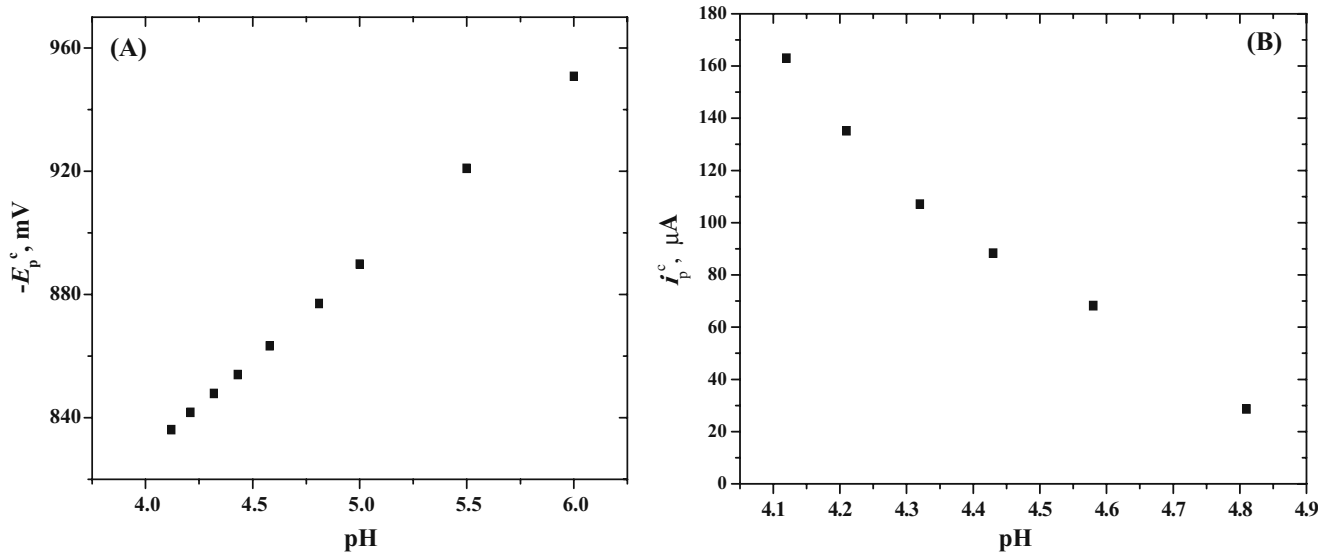

Fig. 17 Variation of the peak potential (**a**) and peak current (**b**) as a function of pH of (1.25 mM) malic acid in a universal buffer on modified GCE with Au_{NPs} at ν=100 mV^{-1} vs. Ag/AgCl

electrodes compared to the bare GCE. Therefore, the results obtained by comparison of the voltammograms and the chemical structure of the investigated compound with oxalic acid and succinic acid indicate that the cathodic wave potential (vs. Ag/AgCl) were also due to reduction of carboxylic group via cleavage of π-bond in the carbonyl group of the carboxylic acid. There is a slight difference in the cathodic peak position of malic, oxalic, and succinic acid, as it is shifted towards the negative direction in the case of malic acid. This difference can be explained on the basis of the presence of the –(CH2–CHOH)-donating groups that hinder the process of electroreduction for malic acid, but less than succinic acid

Dependence of the I_{pc} and E_{pc} of oxalic acid on the pH value The cyclic voltammetric behavior of malic acid was studied as a function of pH. The cyclic voltammograms show similar electrochemical characteristics as (Fig. 16, b). The cathodic peak potential, E_{pc} shifts toward more negative potentials with an increase of pH while simultaneously diminishing in peak current (I_{pc}) height (Fig. 17a, b). The fact that the reduction wave decreases with the pH seems to indicate that the reduction of the radical is preceded by a protonation.

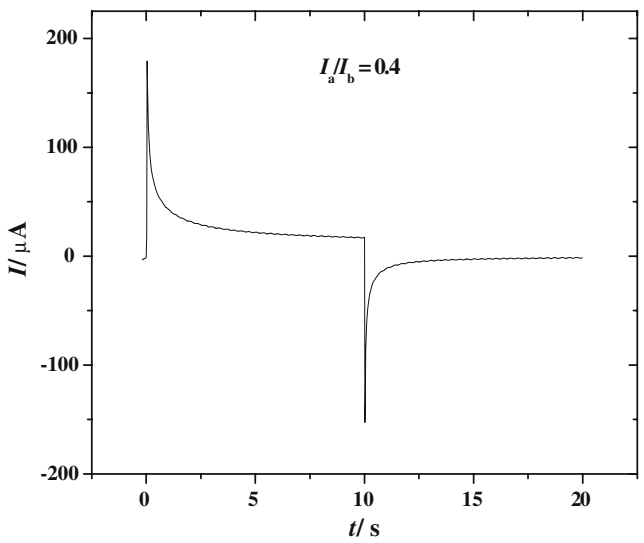

Fig. 18 Double potential step chronoamperogram obtained at GCE modified with Au_{NPs} at load of 8×10^{-5} g cm^{-2}, for 1.25×10^{-3} M malic acid in 0.1 M KCl, at Ei=0 V, Es=−0.88 V, and Ef=0 V, at τ=10 s, at 298 K

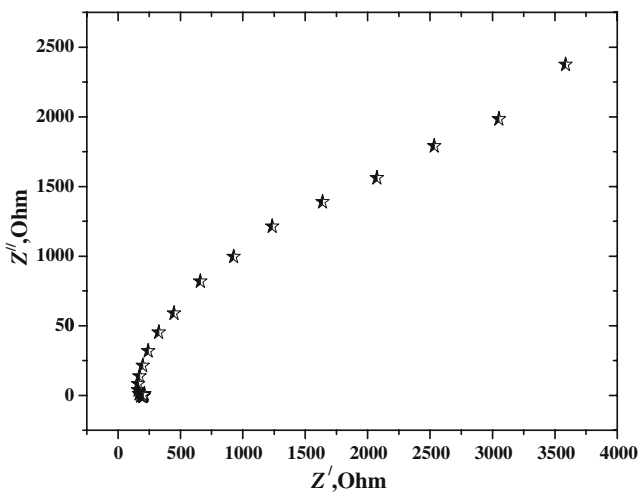

Fig. 19 Complex impedance plane plot at modified with Au_{NPs} at load of 8×10^{-5} g cm^{-2} for solution containing 1.25×10^{-3} M malic acid at the cathodic peak potential vs. Ag/AgCl, in 0.1 M KCl, AC amplitude at 0.005 V. The frequencies from 100 kHz to 5 Hz, at 298 K

Table 7 EIS data was obtained for the electroreduction of 1.25×10^{-3} M malic at the same conditions as in Fig. 19

Electrode	R_s, Ω	R_{ct}, Ω	C_{dl} F$\times10^{-5}$	Φ Angel
Au_{NPs}	199.50	1,050.00	7.22	46.35

The number of protons that participate in the rate determining step have been calculated from Eq. 6. Tafel's slope with respect to malic acid was obtained at potentials corresponding to the foot of the wave ($i/i_p<0.05$). It is found to be 33.3 mV/decade. On the other hand, the variation of E_p, with pH, linear with a slope of −61.4 mV/pH indicates that only two H+ion per acid molecule reduced takes part in the rds. Hence, the electroreduction mechanism of malic acid agree with that has been proposed as oxalic acid.

Double potential step CA

Figure 18 shows the double potential step chronoamperograms at cathodic peak of malic acid. This figure reveals that the I_a/I_b ratio in the case of malic is less than the unity. This is due to the presence of electron transfer process followed by a chemical reaction (EC mechanism).

The diffusion coefficient of malic acid is of the order of 4.46×10^{-5}cm^{2}s^{-1}. The rate of coupled chemical reaction (protonation) of malic acid at the main cathodic peak after the electron transfer process is about ~0.128 s^{-1}. Also, the plot of $It^{1/2}$ vs. t for the cathodic peak of malic shows that $It^{1/2}$ is constant and time-independent. This assumes the diffusionally controlled electron transfer process.

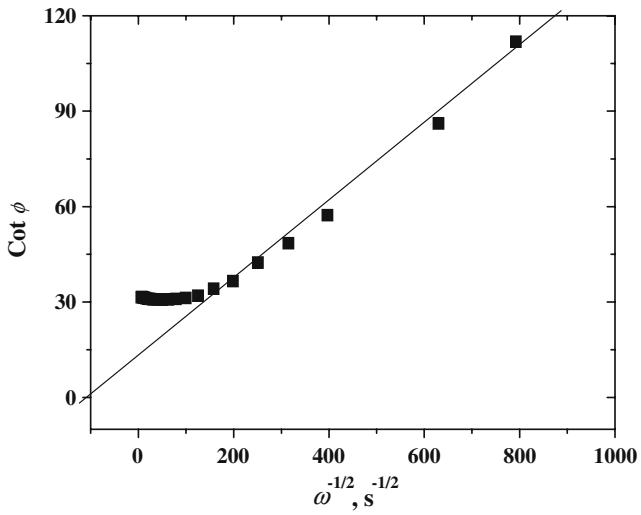

Fig. 20 Dependence of the faradic phase angel on the square root of angular frequency, derived from EIS data, was measured for 1.25×10^{-3}M malic the cathodic peak potential vs. Ag /AgCl, in 0.1 M KCl at Au_{NPs} at load of 8×10^{-5} g cm^{-2} at 298 K

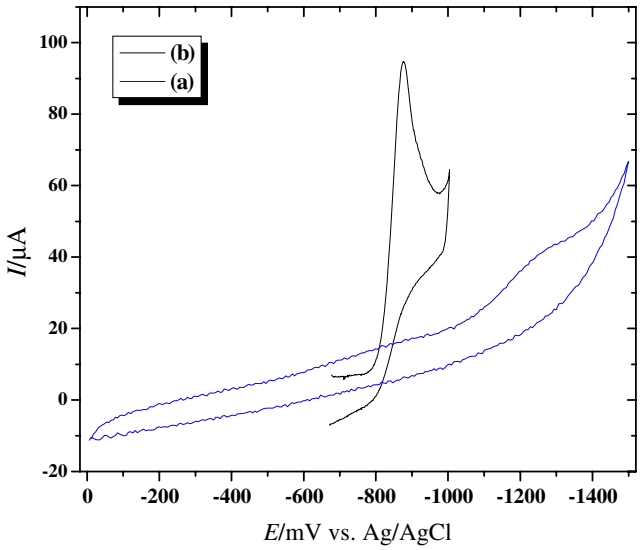

Fig. 21 CV of 1.25×10^{-3}M tartaric acid in 0.1 M KCl on bare GCE (*a*) and modified GCE with Au_{NPs} at load of 8×10^{-5}g cm^{-2} (*b*), at ν= 0.1 Vs^{-1} at 298 K

EIS

Figure 19 shows the Nyquist plot of the impedance spectroscopy on the modified Au nanoparticles electrode for malic, measured from 6.31 Hz to 100 kHz at the cathodic potential peak for malic. The Randles equivalent circuit is not sufficient for the description of this case; thus, it should be assumed the presence of an additional impedance contribution connected with a coupled chemical reaction following the electron transfer process as in the cases of the obvious acids. The extracted parameters for the circuit elements are summarized in Table 7. The R_{ct} in the case of malic acid is considerably small, but higher than oxalic acid, so the C_{dl} relatively high but less than oxalic and more than succinic acid. This can be interpreted on the basis that the electron transfer process in the electroreduction of malic acid is easy to occur but less than oxalic acid and more than succinic acid. Moreover, the straight line at high frequency has not the unity slope. This reveals

Table 8 CV data for the electroreduction of 1.25 mM tartaric acid on the GCE/ Au_{NPs} in 0.1 M KCl at 298 K

Scan rate (mVs^{-1})	$-Ep^c$ (V)	i_{pc} (μA)	$E_{p/2}-E_p$ (mV)	$i_p/\nu^{1/2}$ (μAmV^{-1}s$^{1/2}$)
50	0.875	52.20	28	7.3822
100	0.878	68.80	28.9	6.8800
200	0.890	92.45	29.4	6.5372
300	0.899	110.3	30.7	6.3682
400	0.905	125.90	30.3	6.2950
500	0.910	138.5	31.7	6.1939

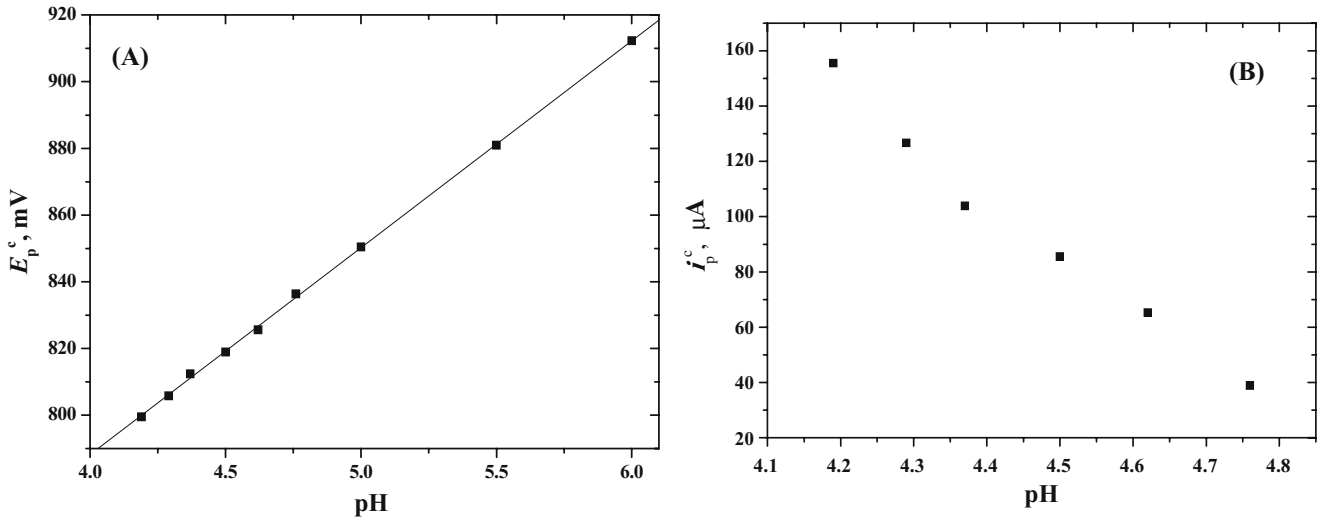

Fig. 22 Variation of the peak potential (**a**) and peak current (**b**) as a function of pH of (1.25 mM) tartaric acid in a universal buffer on modified GCE with Au_{NPs} at ν=100 mV^{-1} vs. Ag/AgCl

that the process is electron transfer combined with a chemical reaction (EC mechanism). The dependence of the angular frequency on cot ϕ as in Fig. 20 shows that lot of points deviate from the detected line and there are points arranged to form another straight line, indicating the presence of an EC process.

Heterogeneous rate of electron transfer reaction for the electroreduction of malic acid at the main cathodic peak was obtained, having value of ~0.09 cm s^{-1}. This value is nearly consistent with those obtained from CV measurements and within the range of the diffusion-controlled processes confirmed with CV and CA measurements.

Electrochemical response of malic acid on the Au nanoparticle-modified electrode

CV

The electrochemical behavior of tartaric acid in aqueous media was qualitatively studied by cyclic voltammetry. The CV investigations indicated that the Au_{NPs} improve the electroreduction behavior of tartaric acid. When the modified GCE/Au_{nano} electrode was used in solution containing tartaric acid, a large increase in cathodic CV current was observed at about −0.87 V (Fig. 21, b).

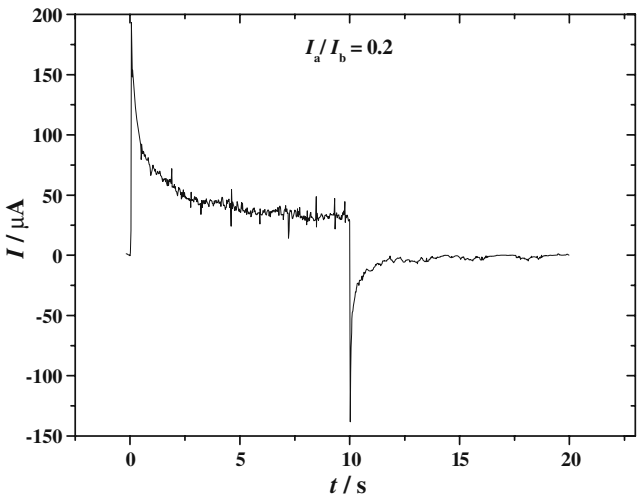

Fig. 23 Double potential step chronoamperogram obtained at GCE modified with Au_{NPs} at load of 8×10^{-5}g cm^{-2}, for 1.25×10^{-3}M tartaric acid in 0.1 M KCl, at Ei=0 V, Es=−0.88 V, and Ef=0 V, at τ= 10 s, at 298 K

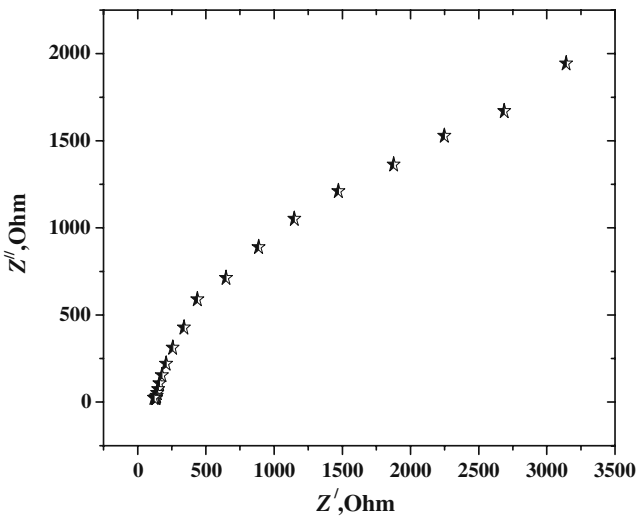

Fig. 24 Complex impedance plane plot at modified with Au_{NPs} at load of 8×10^{-5}g cm^{-2} for solution containing 1.25×10^{-3}M tartaric acid at the cathodic peak potential vs. Ag/AgCl, in 0.1 M KCl, AC amplitude at 0.005 V. The frequencies from 100 kHz to 5 Hz, at 298 K

Table 9 EIS data was obtained for the electroreduction of 1.25×10^{-3}M tartaric at the same conditions as in Fig. 24

Electrode	R_s, Ω	R_{ct}, Ω	C_{dl}F$\times10^{-5}$	Φ Angel
Au_{NPs}	136.46	1,038.45	7.59	43.53

However, when the bare GCE electrode was used in solution containing tartaric acid, no electrochemical reaction could be observed between the potential range from 0.00 to −1.50 V (Fig. 21, a). The cathodic peak potentials, peak currents, peak separations, and current functions for the electroreduction of tartaric acid on GCE modified with Au nanoparticles are summarized in Table 8.

Peak separations confirm that there is a totally irreversible two electron transfer process at the cathodic peak according to the relation (Eq. 5). Also, there is a cathodic shift in peak potential of about ~35 mV for each tenfold increase in the rate of potential scan.

A linear increase relation between the peak current (I_P) and the square root of the scan rate reveals that the electron transfer process was controlled via diffusion phenomena. Also, a linear increase in the peak heights proportional to increase in concentrations of the acid under investigation at millimolar levels (i.e., 1×10^{-3} to 8×10^{-3}M) was observed. Similarly, it confirms that the electron transfer process was also controlled via diffusion phenomena.

Current functions ($i_p/\nu^{1/2}$) decrease with increasing the scan rate (Table 8). This indicates that there is a chemical reaction along with the electron transfer process (EC mechanism) at the electroreduction of tartaric acid.

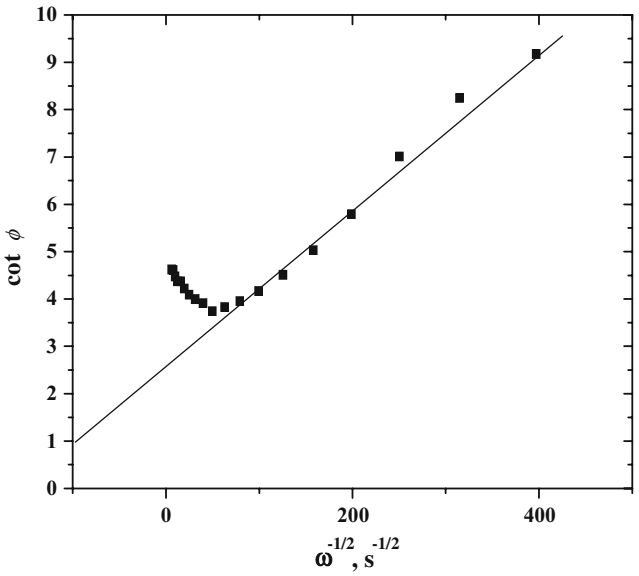

Fig. 25 Dependence of the faradic phase angel on the square root of angular frequency, derived from EIS data, was measured for 1.25×10^{-3}M tartaric at the cathodic peak potential vs. Ag /AgCl, in 0.1 M KCl at Au_{NPs} at load of 8×10^{-5}g cm^{-2} at 298 K

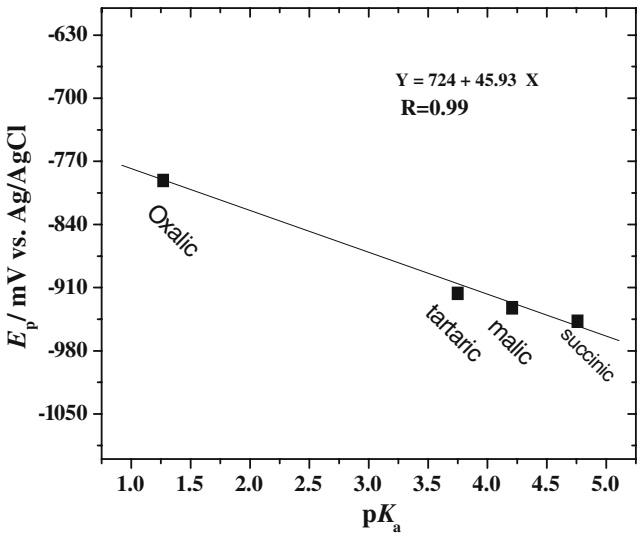

Fig. 26 Linear correlation between pK_{a1} of 1.25 mM for the selected acids and their cathodic peak potentials on modified GCE with Au_{NPs} in 0.1 M KCl at ν=100 mV s^{-1}

Heterogeneous charge transfer rate constant (k_s) for the electroreduction of tartaric acid has a value amounting to ~0.110 cm s^{-1}, assuming $\alpha\approx0.5$ indicating that the reaction is fast on the modified gold nanoparticles electrode and also reflect the facile nature of the charge transfer at the Au_{NPs} electrodes compared to the bare GCE. Therefore, the results obtained by comparison of the voltammograms and the chemical structure of the investigated compound with oxalic acid, succinic acid, and malic acid indicate that the cathodic wave potential (vs. Ag/AgCl) were also due to reduction of carboxylic group via cleavage of π-bond in the carbonyl group of the carboxylic acid. There is a slight difference in the cathodic peak position of tartaric acid from malic, oxalic, and succinic acids, as it is shifted towards to the negative direction compared to oxalic and shifted towards to the positive direction compared to malic and succinic acids. This difference can be explained on the basis of the presence of the $-(CHOH)_2-$ group that affect the process of electroreduction for tartaric acid.

Table 10 Voltammetric peak potentials and the energies of the molecular orbitabels of the studied acids

Acid	$-E_p$, V	E_{HOMO}, eV	E_{LUMO}, eV
Acetic	0.954	−11.1477	1.099
Formic	0.930	−11.8109	1.679
Oxalic	0.791	−11.6096	−0.514
Succinic	0.933	−7.9584	−0.403
Malic	0.880	−9.5474	0.564
Tartaric	0.878	−11.4093	−0.403
Citric	0.845	−11.041	0.0863

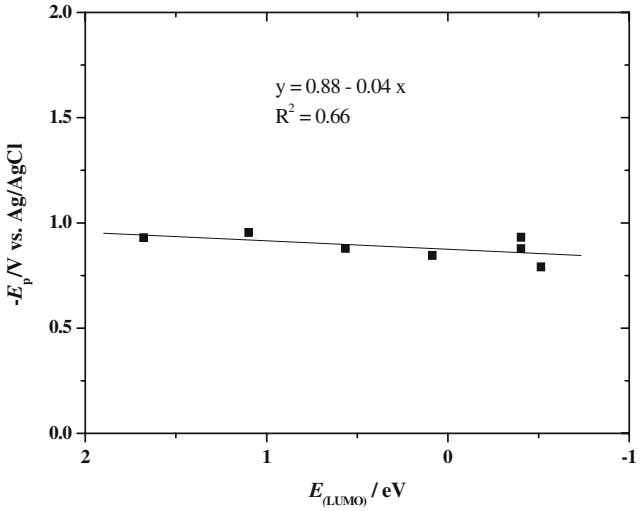

Fig. 27 The dependence of the reduction peak potential on, *E*pc, of the acids present in Table 8 on the energy of the lowest unoccupied orbitals, $E_{(LUMO)}$

Dependence of the Ipc and Epc of oxalic acid on the pH value CV measurements were also carried out by varying the pH of the buffered solutions, and the obtained typical CVs are shown in the inset of Fig. 21, b. As the solution pH was increased, the cathodic peak of tartaric acid gradually shifted to the more negative potential in the pH range of 4.0–6.0. While simultaneously diminishing in peak current (I_{pc}) height (Fig. 22a, b). The observed pH dependence of the cathodic peak potential values of tartaric acid is ascribed to the involvement of protons in the rate-determining step of the electroreduction processes.

The number of protons that participate in the rate determining step have been calculated from Eq. 6. Tafel's slope with respect to tartaric acid was obtained at potentials corresponding to the foot of the wave (i/i_p<0.05). It is found to be 31.3 mV/decade. On the other hand, the variation of E_p, with pH, linear with a slope of −62 mV/pH indicates that only two H+ion per acid molecule reduced takes part in the rds. Hence, the electroreduction mechanism of tartaric acid agree with that has been proposed as oxalic acid.

Double potential step CA

Figure 23 shows the double potential step chronoamperograms at cathodic peak of tartaric acid. This figure reveals that the I_a/I_b ratio in the case of tartaric acid is less than the unity. This is due to the presence of electron transfer process followed by a chemical reaction (EC mechanism). The diffusion coefficient of tartaric acid is found of the order of $5.2\times10^{-5}\,cm^2s^{-1}$.

The rate of coupled chemical reaction (protonation) of tataric acid at the cathodic peak after the electron transfer process is about ~0.124 s^{-1}. The plot of $It^{1/2}$ vs. t for the cathodic peak of tartaric shows that $It^{1/2}$ is constant and time-independent. This assumes the diffusionally controlled electron transfer process.

EIS

Figure 24 shows the Nyquist plot of the impedance spectroscopy on the modified Au_{NPs} electrode for tartaric, measured from 6.31 Hz to 100 kHz at the cathodic potential peak for tartaric. The Randles equivalent circuit is not sufficient for the description of this case; thus, it should be assumed the presence of an additional impedance contribution connected with a coupled chemical reaction following the electron transfer process as in the cases of the obvious acids. The extracted parameters for the circuit elements are summarized in Table 9. The R_{ct} in the case of tartaric acid is considerably small but higher than oxalic acid, so the C_{dl} relatively high but less than oxalic and more than malic and succinic acid. This can be interpreted on the basis that the electron transfer process in the electroreduction of tartaric acid is easy to occur but less than oxalic acid and more than malic and succinic acid. Moreover, the straight line at high frequency has not the unity slope. This reveals that the process is electron transfer combined with a chemical reaction (EC mechanism).

The dependence of the angular frequency on cot ϕ as in Fig. 25 shows that lot of points deviate from the detected line, and there are points arranged to form another straight line, indicating the presence of an EC process. The

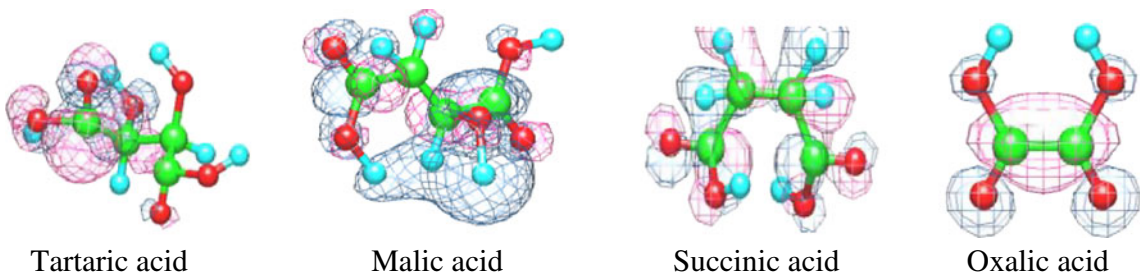

Fig. 28 Molecular structure of the particular acids after a geometric optimization procedure using the program AM1 of winMOPAC 2.0

heterogeneous rate of electron transfer reaction for the electroreduction of tartaric acid at the cathodic peak was obtained, having value of ~0.29 cm s^{-1}. This value is nearly consistent with those obtained from CV measurements and within the range of the diffusion-controlled processes confirmed with CV and CA measurements.

Relationship between Ep and pK_a

Since the electroreduction mechanism of the carboxylic acids under investigation involves protons, the E_{pc} is suggested as a voltammetric parameter to correlate with pK_{a1} values in aqueous media. So, this relation can be used to estimate the pK_{a1} of a new acid from the corresponding E_{pc}. It turns out to be possible to use the main reduction process to simplify the situation for the practical application proposed in this study. Figure 26 shows the plots of E_{pc} against pK_{a1} obtained in aqueous media. As long as the acids have the same functional group, there is a linear relationship between E_{pc} and the pK_{a1} obtained in aqueous media. But acids with different groups exhibit different slopes. When E_p data are plotted against pK_{a1} in corresponding media, good straight line with correlation coefficients (R^2) of 0.99 is observed irrespective of the functional groups of the acids as shown, in Fig. 26. The slope is 0.046 V per pK_{a1} unit. This confirms the fact that the acids under investigation have the same electroreduction mechanism.

Relationship between E_p and the lowest unoccupied molecular orbital energies

The energies of the molecular orbitals have been calculated (Table 10) using the program AM1 of winMOPAC 2.0 [44]. It is found that the peak potentials E_{pc} (V) of the given acids depend linearly on the calculated energy of the lowest unoccupied molecular orbitls E_{LUMO} eV(Figs. 27 and 28).

There seems to exist a weak linear dependence, corresponding to the following:

$$E_{pc}(\mathrm{V}) = 0.04\ E_{(\mathrm{LUMO})} - 0.88 \qquad (11)$$

This equation can help for estimation the reduction potential for new derivatives of these compounds and vice versa.

Conclusions

1. The modified GC electrodes with Au nanoparticles were prepared in our laboratory by easy and fast method, for the electroreduction of the investigated carboxylic acids that have significant biological and industrial importance.
2. The prepared electrodes were investigated and examined by different tools. SEM analysis showed the electrodeposited Au particles in the range of nanometer size.
3. The size and density of the electrodeposits increase by increasing the electrodeposition, the delay time, and the concentration.
4. CV, CA, and EIS measurements reveal the high catalytic activity of the prepared electrodes.
5. The electroreduction of the carboxylic acids under investigation on the modified electrode with Au nanoparticles is much more improved than that on the bare GCE.
6. CV, CA, and EIS measurements confirm that the electroreduction of the acids proceeds via EC.
7. The magnitude of the potential shift caused by the presence of the acids showed a good linear relationship with the acid dissociation constants, pK_a, in the corresponding media.
8. From the molecular orbital calculations, we can estimate the electroreduction potential and/or the E_{LUMO} of a wide range of these derivatives of the acids.

References

1. Haruta M (1997) Catal Today 36:153
2. Grunwaldt JD, Kiener C, Wogerbauer C, Baiker A (1999) J Catal 181:223
3. Boccuzzi F, Chiorino A, Manzola M (2001) Mater Sci Eng C 15:215
4. Finot MO, Braybrook GD, Mcdermott MT (1999) J Electroanal Chem 466:234
5. Finot MO, McDermott MT (2000) J Electroanal Chem 488:125
6. Daniel MC, Astruc D (2004) Chem Rev 104:293
7. Georgolios N, Jannakoudakis D, Karabinas P (1989) J Electroanal Chem 264:235
8. Zoval JV, Biernacki PR, Penner RM (1996) Anal Chem 68:1585
9. Zoval JV, Stiger RM, Biernacki PR, Penner RM (1996) J Phys Chem 100:837
10. Zoval JV, Lee J, Gorer S, Penner RM (1998) J Phys Chem B 102:1166
11. Chen Z, Li J, Wang E (1994) J Electroanal Chem 373:83
12. Yoon BU, Cho K, Kim H (1996) Anal Sci 12:321
13. Dekanski A, Stevanovic J, Stevanovic R, Nikolic BZ, Jovanovic VM (2001) Carbon 39:1195
14. Martel D, Kuhn A (2000) Electrochim Acta 45:1829
15. Ye JH, Fedkiw PS (1996) Electrochim Acta 41:221
16. Sarapuu A, Tammeveski K, Tenno TT, Sammelselg V, Kontturi K, Schiffrin DJ (2001) Electrochem Commun 3:446
17. Carralero VS, Mena ML, Gonzalez-Cortes A, Yanez P, Sedeno K, Pingarron JM (2005) Anal Chim Acta 528:1
18. Lund H, Hammerich O (1991) Organic electrochemistry. Marcel Dekker, New York
19. Yang-Liu Zhou, Xin-Sheng Zhang, Ying-Chun Dai, Wei-Kang Yuan (2003) Chem Eng Sci 58:1021

20. Stephen Treimer E, Dennis Evans H (1998) J Electroanal Chem 449:39
21. Trejo G, Gil AF, Gonzalez I (1995) J Electrochem Soc 142:3404
22. Schmidt U, Donten M, Osteryoung JG (1997) J Electrochem Soc 144:2013
23. Xiao-Hong X, Charles Husse L (1992) J Electrochem Soc 139:3108
24. El-Deab MS, Okajima T, Ohsaka AT (2003) J Electrochem Soc 150:A851
25. Trasatti S, Petrii OA (1991) Pure Appl Chem 63:711
26. El-Deab MS, Sotomura T, Ohsaka T (2005) Electrochem Commun 7:29
27. Gopalan AL, Lee KP, Manesh KM, Santhosh P, Kim JH (2006) Catal Chem 256:335
28. Forker W (1989) Electrochemistry. Akademie, Berlin
29. Lu Y, Yang M, Qu F, Shen G, Yu R (2007) Bioelectrochemistry 71:211
30. Hrapovic S, Lui Y, Male KB, Luong JHT (2004) Anal Chem 76:1083
31. Bard AJ, Faulkner LR (2001) Electrochemical methods fundamentals and applications. Wiley, New York
32. Nicholson RS, Shain I (1964) Anal Chem 36:706
33. Marcus RA (1965) J Chem Phys 43:679
34. Greef R, Peat R, Peter LM, Pletcher D, Robinson J (1985) Instrumental method in electrochemistry. Ellis Horwood, Chichester
35. Hu IF, Karweik DH, Kuwana T (1985) J Electroanal Chem 188:59
36. Zhang S, Wang N, Niu Y, Sun C (2005) Sens Actuators B Chem 109:367
37. Lin WZ, Yi L, Ze Z (2003) Handbook of nanophase and nanostructured materials. Kluwer, New York
38. Zhang L, Jiang X, Wang E, Dong S (2005) Biosens Bioelectron 21:337
39. Gimenez I, Diard JP, Maximovitch BLGS (1988) Electrochim Acta 33:137
40. Farzinnejad N, Miran Beigi AA, Fotouhi L, Torkestani K, Ghadirian HA (2005) J Electroanal Chem 580:245
41. Schwarz WM, Shain I (1965) J Phys Chem 69:30
42. Rashwan F, Mohran H (1993) Bull Chem Soc Jpn 66:1871
43. Pospisil L, SoKolova R, Colombini MP, Giannarelli S, Fuoco R (2000) Microchem J 67:305
44. Stewart JJP (1998) WinMOPAC 0.2, user manual. Fujitsu, Tokyo